# Electronic structure of III-V zinc-blende semiconductors from first principles

Yin Wang,[1,*] Haitao Yin,[1,2,†] Ronggen Cao,[1,3,‡] Ferdows Zahid,[1] Yu Zhu,[4] Lei Liu,[4] Jian Wang,[1] and Hong Guo[1,5]

[1]*Department of Physics and the Center of Theoretical and Computational Physics, The University of Hong Kong, Pokfulam Road, Hong Kong SAR, China*

[2]*Key Laboratory for Photonic and Electronic Bandgap Materials of Ministry of Education, School of Physics and Electronic Engineering, Harbin Normal University, Harbin 150025, China*

[3]*Department of Materials Science, Fudan University, Shanghai 200433, China*

[4]*Nanoacademic Technologies, Brossard, PQ, Canada, J4Z 1A7*

[5]*Center for the Physics of Materials and Department of Physics, McGill University, Montreal, PQ, Canada, H3A 2T8*

(Received 29 March 2013; revised manuscript received 21 May 2013; published 10 June 2013)

For analyzing quantum transport in semiconductor devices, accurate electronic structures are critical for quantitative predictions. Here we report theoretical analysis of electronic structures of all III-V zinc-blende semiconductor compounds. Our calculations are from density functional theory with the semilocal exchange proposed recently [Tran and Blaha, Phys. Rev. Lett. **102**, 226401 (2009)], within the linear muffin tin orbital scheme. The calculated band gaps and effective masses are compared to experimental data and good quantitative agreement is obtained. Using the theoretical scheme presented here, quantum transport in nanostructures of III-V compounds can be confidently predicted.

DOI: 10.1103/PhysRevB.87.235203 PACS number(s): 71.15.Mb, 71.55.Eq, 71.15.Ap

## I. INTRODUCTION

During the past five decades, semiconductor device miniaturization has brought modern device technology to the nanometer scale where quantum phenomena of charge and spin transport start to dominate the device physics.[1,2] For tiny devices, the atomic nature of the materials is playing an increasingly prominent role[1] and charge transport in these systems driven by external fields is intrinsically a nonequilibrium problem. As a result the operation of nanoscale electronics crucially depends on the close coupling of nonequilibrium quantum transport phenomena with the atomic structure of the device material. Such a situation poses serious challenges to theoretical understanding and computational modeling of nanoelectronic device physics. More recently, atomistic methods have been combined with the Keldysh nonequilibrium Green's function (NEGF) formalism[3,4] to meet the challenges of quantitative analysis of nanoelectronics. The atomistic methods are used to determine the material properties as well as the device Hamiltonian while NEGF is used to predict the nonequilibrium density matrix and transport properties. When combined self-consistently, such techniques can predict not only qualitative but also quantitative properties of quantum transport in nanodevices. Along this line, the state-of-the-art formalism is to carry out self-consistent density functional theory (DFT)[5] atomistic calculation within the NEGF framework.[4] So far, parameter-free NEGF-DFT methods have been widely applied to capture quantum transport physics from the atomistic point of view.[6]

However, in order to apply a first principles approach to investigate *semiconductor* nanoelectronics, some very serious issues have to be resolved. First, realistic semiconductor devices (e.g., transistors) have a large number of atoms and are doped with small concentrations of impurities, while typical DFT methods can only comfortably deal with low hundreds of atoms. Second, DFT with the local density approximation (LDA)[7–9] and generalized gradient approximation (GGA)[10,11] underestimates band gaps of semiconductors. One could not predict transport results if band gaps and dispersions were not accurate; this is especially serious for semiconductors appearing in transistors since their gaps are not very large to begin with. Advanced methods such as $GW$[12] and hybrid functionals[13] can yield accurate band gaps for many systems, but require very large computation for semiconductor devices having hundreds to thousands of atoms.

For pure semiconductors, a recently proposed modified Becke-Johnson (MBJ) semilocal exchange[14] was shown to give good band gaps for many semiconductors, especially for *sp* bond systems,[15] with a computational cost similar to that of LDA. MBJ is not a fundamental solution to the issue of electron correlation, but it is practically useful for calculating band structures and thus helpful for analyzing quantum transport properties. By implementing the MBJ functional into a newer generation of NEGF-DFT technique which is based on the linear muffin tin orbital (LMTO) method with the atomic sphere approximation (ASA),[16] transport in Si nanotransistors with localized doping and large number of atoms was recently analyzed.[17] Clearly, a very important next step is to investigate III-V semiconductors.

The III-V compound semiconductors are the most important materials for optoelectronic device applications[18] and are also very important for the complementary metal-oxide-semiconductors (CMOS) technology. Major efforts are devoted by the microelectronics industry to integrate III-V semiconductors into Si CMOS.[19] III-V semiconductors have been extensively investigated both experimentally and theoretically,[20–24] with particular attention paid to their band topologies since band parameters are critical for understanding quantum transport. Recently, electronic structures of several direct gap III-V compounds have been calculated using the MBJ functional as implemented in plane-wave DFT codes,[24] and the calculated band gaps are significantly more accurate than reported previously.[20,21,23] We note, however, that a plane-wave basis is more difficult to apply for nonequilibrium quantum transport calculations as it produces prohibitively

 

TABLE I. The lattice constant $\alpha$ of the III-V compounds and the $c$ values used in the DFT-MBJ calculations. $c_{\text{atom}}$ and $c_{\text{vac}}$ are the $c$ values for real atoms and the vacancy spheres, respectively.

| Material | $\alpha$ (Å) | $c_{\text{atom}}$ | $c_{\text{vac}}$ | Material | $\alpha$ (Å) | $c_{\text{atom}}$ | $c_{\text{vac}}$ |
|---|---|---|---|---|---|---|---|
| GaAs | 5.6533 | 1.20 | 1.39 | GaP | 5.4505 | 1.13 | 1.50 |
| AlAs | 5.6611 | 1.11 | 1.44 | AlP | 5.4672 | 0.69 | 1.44 |
| InAs | 6.0583 | 1.18 | 1.00 | InP | 5.8697 | 1.04 | 1.39 |
| GaSb | 6.0959 | 1.17 | 1.23 | GaN | 4.50 | 1.19 | 1.50 |
| AlSb | 6.1355 | 1.12 | 1.33 | AlN | 4.38 | 1.59 | 1.55 |
| InSb | 6.4794 | 1.19 | 0.62 | InN | 4.98 | 1.56 | 1.39 |

large and dense matrices when it comes to constructing Green's functions. Indeed, first-principles quantum transport calculations are typically done with localized basis such as LCAO[4] and LMTO.[25,26] Motivated by this fact and by the importance of III-V materials in nanoelectronic devices, it is the purpose of this work to employ the MBJ semilocal exchange within the DFT-LMTO approach to accurately calculate the band parameters of *all* the zinc-blend III-V semiconductors. Our calculated band gaps at high-symmetry points ($\Gamma$, $X$, and $L$) are quantitatively compared with the corresponding experimental data; our calculated effective hole/electron masses at the $\Gamma$ point are also very consistent with the experimental values. These results indicate that quantum transport properties of III-V nanostructures can be well predicted from first principles using the MBJ semilocal exchange witin the DFT-LMTO method. Finally, details of the LMTO-ASA schemes and the MBJ potentials will also be presented.

The rest of the paper is organized as follows. In the next section the calculation method is briefly discussed. Section III presents the results and Sec. IV is a short summary.

## II. METHOD

Our calculation is based on the DFT-MBJ self-consistent approach where DFT is within the LMTO scheme and the atomic sphere approximation,[25] as implemented in the NANODSIM software package.[16] For technical details of the NANODSIM algorithm we refer interested readers to the original literature.[16,26] A $12 \times 12 \times 12$ $k$-mesh was used to sample the Brillouin zone of the primitive cell. The lattice constant for the semiconductors was adopted from Ref. 20 and listed in Table I. In order to carry out LMTO DFT calculations for semiconductors, a good ASA scheme is very helpful. In our ASA, we follow Ref. 27 to add vacancy spheres for space filling. Note that the same sphere radius is used for both vacancy sphere and atomic sphere. Electrons in the full $d$ orbital of Ga, In, As, and Sb are included as valence electrons. After the LMTO DFT self-consistent calculation is completed, band structures are calculated by the the muffin-tin orbital (MTO) approach. The effective hole mass $m_h^*$ and effective electron mass $m_e^*$ were then obtained by fitting the valence band maximum and conduction band minimum to a parabola, respectively. Spin-orbit coupling was not considered in this work.

Following Ref. 14, the MBJ potential is

$$v_{x,\sigma}^{MBJ}(r) = c v_{x,\sigma}^{BR}(r) + (3c-2)\frac{1}{\pi}\sqrt{\frac{5}{12}}\sqrt{\frac{2t_\sigma(r)}{\rho_\sigma(r)}}, \quad (1)$$

where subscript $\sigma$ is spin index, and $\rho_\sigma$ is the electron density for spin channel $\sigma$. The quantity $t_\sigma$ is the kinetic energy density and $v_{x,\sigma}^{BR}(r)$ is the Becke-Roussel potential of Ref. 28. The above MBJ potential has two terms whose relative weight is given by a parameter $c$. It was shown in Ref. 14 that the value of $c$ depends linearly on the square root of the average of $|\nabla\rho|/\rho$. It appears that $E_g$ increases monotonically with $c$.[14] The value of $c$ for each compound can be determined by the protocol discussed in Refs. 14 and 29. In our calculations, because the LMTO-ASA is a site-oriented technique, it allows the $c$ value to be "local"; namely one can use different $c$ values for different real atom/vacancy spheres. In particular, for a given compound, the same $c$ value is used for the real atoms (e.g., Ga and As), and another $c$ value is used for the vacancy spheres. Recently, this MBJ scheme was applied in Ref. 30 to determine accurate band gaps for the $Al_xGa_{1-x}As$ compounds and reasonable band offsets for the GaAs/$Al_xGa_{1-x}As$ heterojunctions for the entire range of the concentration $0 \leqslant x \leqslant 1$. Here we use the same scheme[30] for all the III-V compounds; namely, we fix the $c$ parameter to values that best reproduce experimental band gaps for each compound. These optimized $c$ values are listed in Table I. Even though one may expect more accurate band gaps by using different optimized $c$ values for all the different atomic spheres, the scheme we use is a good compromise between being simple and also reasonably accurate.

## III. RESULTS

We begin by calculating the band structures of the III-V compounds with LDA[7] using the projector augmented waves (PAW) method and a plane-wave basis set of 400 eV cutoff, as implemented in the Vienna *Ab initio* Simulation Package (VASP),[31] as well as using the DFT-LMTO method discussed in the last section where the ASA scheme follows that of Ref. 27, as implemented in the NANODSIM[16] NEGF-DFT package. The LDA results of the two method for all the zinc-blende III-V compounds are plotted in Fig. 1. While the two curves almost overlap perfectly in the figures, we can quantify the difference of the two results (red line from PAW and blue circles from LMTO) by calculating their relative deviations. For instance, the relative deviation at the $\Gamma$, $X$, and $L$ points of the valence band maxima for GaAs between the results by PAW and LMTO are 0%, 0.04%, and 2.02%; the deviations at the corresponding conduction band minima are 0.60%, 5.90%, and 5.61%. In the same fashion, we calculated the relative deviations between the PAW and LMTO methods at the $\Gamma$, $X$, and $L$ points for all the compounds to deduce an average

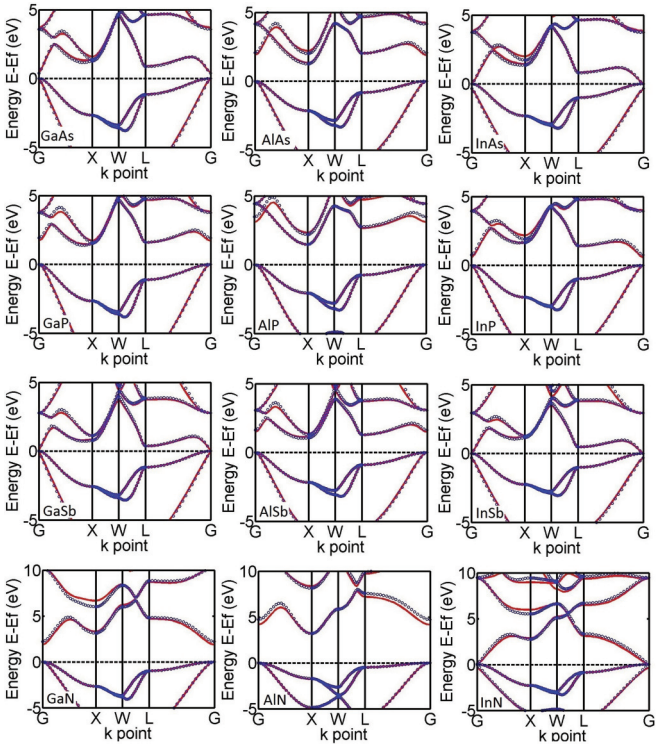


FIG. 1. (Color online) The band structures for the III-V compound semiconductors obtained with LDA. Red line is obtained by VASP (PAW), blue circles obtained by NANODSIM (LMTO).

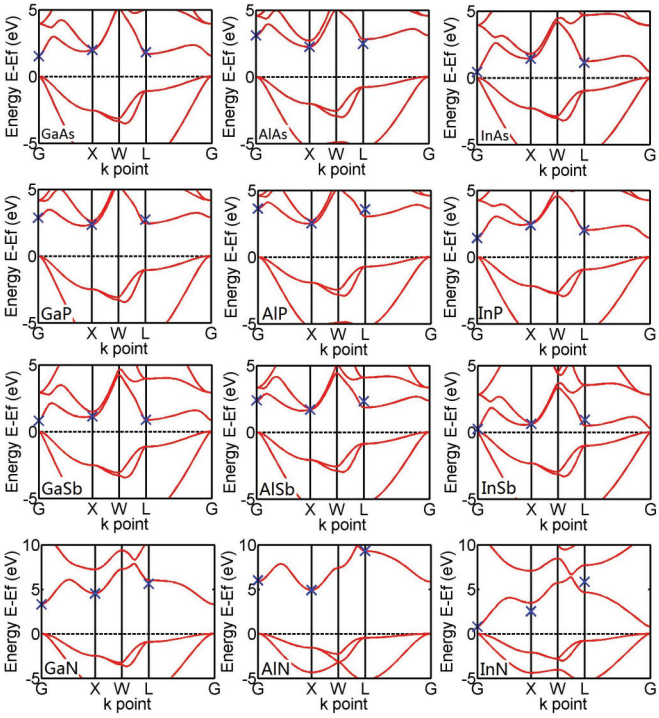


FIG. 2. (Color online) The band structures for the III-V compound semiconductors obtained with MBJ as implemented in the DFT-LMTO scheme. Blue crosses indicate the experimental values.

deviation for the III-V materials as a whole (i.e., average over all the III-V compounds). For the valence band maxima, almost perfect agreement is obtained for the two methods where the average deviations are 0%, 1.46%, and 1.28% at the Γ, $X$, and $L$ points, respectively. For the conduction band minima, a good agreement is obtained for the two methods where the average deviations are 15.16%, 4.58%, and 3.92% at the Γ, $X$, and $L$ points. The agreement of the two methods is quite respectable for the III-V materials as a whole.[32] Such an agreement between PAW and LMTO-ASA suggests that our ASA scheme is accurate for calculating physical properties of these materials.

It should be noted from Fig. 1 that the band gaps were underestimated by LDA. Having confirmed our ASA scheme, we next apply the MBJ functional[14,29] to calculate the electronic structure again using the LMTO-ASA approach, and the MBJ results are plotted in Fig. 2. Compared with the LDA bands in Fig. 1, the opening of band gaps is evident. From Fig. 2, the band gap values at the Γ, $X$, and $L$ points are obtained and listed in the third column of Table II. In Ref. 24, five direct gap compounds were calculated with the MBJ functional within a plane-wave method; their band gap values are also listed in Table II in the fourth column. Our results for these five compounds agree well with the plane-wave results except for the $X$ point of InAs and $X, L$ points of InSb. As discussed in Ref. 24, for these narrow-band semiconductors, it is difficult to accurately determine the gaps at the $X$ point. For instance, an experimental gap value of 0.63 eV was recommended for InSb in Ref. 20 but other values such as 1.80 eV were also reported in earlier literature.[33] For InSb, our gap values at the Γ, $X$ points are in good agreement with experimental results, while the plane-wave gap values at the Γ, $L$ points agree well with the experiments. This difference is due to the use of different $c$ values in the MBJ potential in the LMTO-ASA and the plane-wave calculations. As a whole the consistency of MBJ results from the two methods is satisfactory.

The experimental gap values are taken from Refs. 20 and 21 and listed in the fifth column in Table II. The last column is the percentage difference between our calculated values and the experimental values. Of the 36 tabulated gap values, 32 of them are in good agreement with the experimental data. There are 4 values having a difference over 20%: the $L$ point of InSb, the $X$ and $L$ points of InN, and the $L$ point of AlSb. These differences could be due to the uncertainties of the experimental values for the narrow gap compounds InSb and InN[24] and, of course, the approximative nature of the DFT calculations. Nevertheless, it is impressive that, all in all, the MBJ band gaps are in good consistency with the experimental values for this wide range of materials.

From the calculated band structures shown in Figs. 1 and 2, we obtain the effective masses of electrons and holes by fitting the valance band maximum or conduction band minimum to a parabola at the Γ point along the [100] direction; the results are listed in Table III together with the experimental values.[20,21] The deviation of our calculated values from the experimental values is also listed for each compound. For the MBJ results, good agreement is obtained for most situations except for AlN and the electron effective mass of GaN. Given the fact that effective masses are usually very hard to determine accurately, the good consistency to the experimental results for most situations is satisfactory. In the same table, we also list our

TABLE II. Energies of the conduction band minima (band gaps, $E_g$) at the Γ, $X$, and $L$ points with respect to the valence band maximum at the Γ point in units of eV, calculated by the DFT-MBJ approach at zero temperature. The experimental results are taken from Ref. 20 (except where noted). $MBJ_V$ shows the DFT-MBJ values from Ref. 24. The last column gives the percentage difference of our calculated values from the experimental values.

| Material | $E_g$ | This work | $MBJ_V$[24] | Expt.[20] | Deviation (%) |
|---|---|---|---|---|---|
| GaAs | Γ | 1.529 | 1.52 | 1.519 | 0.7 |
| | $X$ | 2.003 | 2.00 | 1.981 | 1.1 |
| | $L$ | 1.682 | 1.72 | 1.815 | 7.3 |
| AlAs | Γ | 3.087 | | 3.099 | 0.4 |
| | $X$ | 2.240 | | 2.240 | 0 |
| | $L$ | 2.800 | | 2.460 | 13.8 |
| InAs | Γ | 0.416 | 0.43 | 0.417 | 0.2 |
| | $X$ | 1.440 | 2.01 | 1.433 | 0.5 |
| | $L$ | 1.225 | 1.43 | 1.133 | 8.1 |
| GaP | Γ | 2.887 | | 2.886 | 0 |
| | $X$ | 2.350 | | 2.350 | 0 |
| | $L$ | 2.429 | | 2.720 | 10.7 |
| AlP | Γ | 3.635 | | 3.630 | 0.1 |
| | $X$ | 2.513 | | 2.520 | 0.3 |
| | $L$ | 3.030 | | 3.570 | 15.1 |
| InP | Γ | 1.421 | 1.42 | 1.424 | 0.2 |
| | $X$ | 2.502 | 2.34 | 2.384 | 4.9 |
| | $L$ | 2.007 | 2.11 | 2.014 | 0.3 |
| GaSb | Γ | 0.818 | 0.82 | 0.812 | 0.7 |
| | $X$ | 1.117 | 1.21 | 1.141 | 2.1 |
| | $L$ | 0.876 | 0.87 | 0.875 | 0.1 |
| AlSb | Γ | 2.346 | | 2.386 | 1.7 |
| | $X$ | 1.698 | | 1.696 | 0.1 |
| | $L$ | 1.845 | | 2.329 | 20.8 |
| InSb | Γ | 0.238 | 0.25 | 0.235 | 1.3 |
| | $X$ | 0.613 | 1.52 | 0.630 | 2.7 |
| | $L$ | 0.477 | 0.82 | 0.930 | 48.7 |
| GaN | Γ | 3.298 | | 3.299 | 0 |
| | $X$ | 4.528 | | 4.520 | 0.2 |
| | $L$ | 5.997 | | 5.590 | 7.3 |
| AlN | Γ | 5.853 | | 6.0 | 2.5 |
| | $X$ | 4.908 | | 4.9 | 0.2 |
| | $L$ | 9.304 | | 9.3 | 0 |
| InN | Γ | 0.781 | | 0.78[21] | 0.1 |
| | $X$ | 3.456 | | 2.51 | 37.7 |
| | $L$ | 4.635 | | 5.82 | 20.4 |

TABLE III. Effective hole and electron masses at the Γ point in units of the electron rest mass $m_e$ calculated along the [100] direction by DFT-LMTO method within LDA and MBJ. The experimental values are taken from Ref. 20 (except where noted). The deviation columns show the percentage difference of our calculated values from the experimental values.

| Material | Method | $\lvert m_h^* \rvert$ | Deviation (%) | $\lvert m_e^* \rvert$ | Deviation (%) |
|---|---|---|---|---|---|
| GaAs | MBJ | 0.355 | 1.4 | 0.076 | 13.4 |
| | LDA | 0.320 | 8.6 | 0.024 | 64.2 |
| | Expt. | 0.350 | | 0.067 | |
| AlAs | MBJ | 0.510 | 8.1 | 0.149 | 0.7 |
| | LDA | 0.454 | 3.8 | 0.103 | 31.3 |
| | Expt. | 0.472 | | 0.150 | |
| InAs | MBJ | 0.373 | 12.0 | 0.029 | 11.5 |
| | LDA | 0.360 | 8.1 | 0.026 | 0 |
| | Expt. | 0.333 | | 0.026 | |
| GaSb | MBJ | 0.265 | 6.0 | 0.041 | 5.1 |
| | LDA | 0.254 | 1.6 | 0.010 | 74.4 |
| | Expt. | 0.250 | | 0.039 | |
| AlSb | MBJ | 0.367 | 2.8 | 0.118 | 15.7 |
| | LDA | 0.335 | 6.2 | 0.082 | 41.4 |
| | Expt. | 0.357 | | 0.140 | |
| InSb | MBJ | 0.263 | 0 | 0.018 | 28.6 |
| | LDA | 0.289 | 9.9 | 0.022 | 57.1 |
| | Expt. | 0.263 | | 0.014 | |
| GaP | MBJ | 0.411 | 26.1 | 0.163 | 25.4 |
| | LDA | 0.359 | 10.1 | 0.106 | 18.5 |
| | Expt. | 0.326 | | 0.130 | |
| AlP | MBJ | 0.595 | 14.9 | 0.209 | 5.0 |
| | LDA | 0.533 | 2.9 | 0.180 | 18.2 |
| | Expt. | 0.518 | | 0.220 | |
| InP | MBJ | 0.450 | 15.4 | 0.094 | 17.5 |
| | LDA | 0.404 | 24.1 | 0.054 | 32.5 |
| | Expt. | 0.532 | | 0.080 | |
| GaN | MBJ | 0.927 | 8.4 | 0.232 | 54.7 |
| | LDA | 0.840 | 1.8 | 0.179 | 19.3 |
| | Expt. | 0.855 | | 0.15 | |
| AlN | MBJ | 1.587 | 55.6 | 0.319 | 27.6 |
| | LDA | 1.424 | 39.6 | 0.304 | 21.6 |
| | Expt. | 1.020 | | 0.25 | |
| InN | MBJ | 0.977 | 17.3 | 0.085 | 21.4 |
| | LDA | 0.866 | 4.0 | 0.020 | 71.4 |
| | Expt. | 0.833 | | 0.07[21] | |

calculated effective masses by LDA. The LDA *hole* effective masses are seen to agree well with the experimental results. However, most of the LDA *electron* effective masses have a larger discrepancy as compared to experiments than those obtained with the MBJ potential.

## IV. SUMMARY

We have calculated the electronic structures of all zinc-blende III-V semiconductor compounds from density functional theory with the semilocal exchange of the MBJ form,[14] using the LMTO-ASA scheme. In our method and due to ASA, vacancy spheres are added to fill the volume of the semiconductors. Since this is a sited-oriented calculation method, the weight parameter $c$ in the MBJ potential for the atoms and for the vacancy sites is different. We determine the optimal values of this weight parameter for all the compounds. The calculated band gaps are mostly in very good agreement with the corresponding experimental data. The obtained effective masses are also largely in good agreement to the measurements. For analyzing quantum transport in semiconductor nanoelectronics, accurate electronic structures are very important for quantitative predictions. In addition, as we have shown recently, the band offset of heterojunctions can also be accurately predicted using the same method as reported here.[30] Together with the results of this paper, quantum transport properties of III-V systems can now be confidently calculated from the atomic point of view since the LMTO-ASA method can self-consistently calculate very large numbers of atoms.[17]

**ACKNOWLEDGMENTS**

This work is supported by the University Grant Council (Contract No. AoE/P-04/08) of the Government of HKSAR, NSERC (H.G.), IRAP (Y.Z., L.L.) of Canada, and Reserve Talents of Universities Overseas Research Program of Heilongjiang (H.Y.). We thank CLUMEQ for the computation resources.

*yinwang@hku.hk
†wlyht@126.com
‡caoronggen@fudan.edu.cn

[1] International Technology Roadmap for Semiconductors, http://public.itrs.net.
[2] S. Datta, *Electronic Transport in Mesoscopic Systems* (Cambridge University Press, New York, 1995).
[3] A. P. Jauho, N. S. Wingreen, and Y. Meir, Phys. Rev. B **50**, 5528 (1994).
[4] J. Taylor, H. Guo, and J. Wang, Phys. Rev. B **63**, 245407 (2001); **63**, 121104 (2001).
[5] P. Hohenberg and W. Kohn, Phys. Rev. **136**, B864 (1964); W. Kohn and L. J. Sham, *ibid.* **140**, A1133 (1965).
[6] S. Datta, *Quantum Transport: Atom to Transistor* (Cambridge University Press, New York, 2005).
[7] J. P. Perdew and A. Zunger, Phys. Rev. B **23**, 5048 (1981).
[8] D. M. Ceperley and B. J. Alder, Phys. Rev. Lett. **45**, 566 (1980).
[9] S. H. Vosko, L. Wilk, and M. Nusair, Canadian J. Phys. **58**, 1200 (1980).
[10] J. P. Perdew, J. A. Chevary, S. H. Vosko, K. A. Jackson, M. R. Pederson, D. J. Singh, and C. Fiolhais, Phys. Rev. B **46**, 6671 (1992).
[11] J. P. Perdew, K. Burke, and M. Ernzerhof, Phys. Rev. Lett. **77**, 3865 (1996).
[12] L. Hedin, Phys. Rev. **139**, A796 (1965); J. E. Northrup, M. S. Hybertsen, and S. G. Louie, Phys. Rev. Lett. **59**, 819 (1987); C. Petrillo and F. Sacchetti, Phys. Rev. B **38**, 3834 (1988).
[13] J. Heyd, G. E. Scuseria, and M. Ernzerhof, J. Chem. Phys. **118**, 8207 (2003).
[14] F. Tran and P. Blaha, Phys. Rev. Lett. **102**, 226401 (2009).
[15] D. J. Singh, Phys. Rev. B **82**, 205102 (2010).
[16] For recent reviews, see, for example, J. Maassen, M. Harb, V. Michaud-Rioux, Y. Zhu, and H. Guo, Proc. IEEE **101**, 518 (2013); Y. Zhu, L. Liu, and H. Guo, arXiv:1305.2515.
[17] J. Maassen and H. Guo, Phys. Rev. Lett. **109**, 266803 (2012).
[18] K. Alavi, H. Temkin, W. R. Wagner, and A. Y. Cho, Appl. Phys. Lett. **42**, 254 (1983).
[19] T. Li, M. Mastro, and A. Dadgar, *III-V Compound Semiconductors: Integration with Silicon-based Microelectronics* (CRC Press, Boca Raton, FL, 2011).
[20] I. Vurgaftman, J. R. Meyer, and L. R. Ram-Mohan, J. Appl. Phys. **89**, 5815 (2001).
[21] I. Vurgaftman and J. R. Meyer, J. Appl. Phys. **94**, 3675 (2003).
[22] A. Franciosi and C. G. Van de Walle, Surf. Sci. Rep. **25**, 1 (1996).
[23] L. G. Ferreira, M. Marques, and L. K. Teles, Phys. Rev. B **78**, 125116 (2008); A. Belabbes, C. Panse, J. Furthmüller, and F. Bechstedt, *ibid.* **86**, 075208 (2012); A. Dal Corso, *ibid.* **86**, 085135 (2012).
[24] Y. S. Kim, M. Marsman, G. Kresse, F. Tran, and P. Blaha, Phys. Rev. B **82**, 205212 (2010).
[25] I. Turek, V. Drchal, J. Kudrnovský, M. Šob, and P. Weinberger, *Electronic Structure of the Disordered Alloys, Surfaces, and Interfaces* (Kluwer, Boston, 1977); J. Kudrnovský, V. Drchal, and J. Masek, Phys. Rev. B **35**, 2487 (1987).
[26] Y. Ke, K. Xia, and H. Guo, Phys. Rev. Lett. **100**, 166805 (2008); **105**, 236801 (2010); Y. Ke, Ph.D thesis, McGill University, 2010.
[27] M. César, Y. Ke, W. Ji, H. Guo, and Z. Mi, Appl. Phys. Lett. **98**, 202107 (2011).
[28] A. D. Becke and M. R. Roussel, Phys. Rev. A **39**, 3761 (1989).
[29] D. Koller, F. Tran, and P. Blaha, Phys. Rev. B **85**, 155109 (2012).
[30] Y. Wang, F. Zahid, Y. Zhu, L. Liu, J. Wang, and H. Guo, Appl. Phys. Lett. **102**, 132109 (2013).
[31] G. Kresse and J. Hafner, Phys. Rev. B **47**, 558 (1993); G. Kresse and J. Furthmuller, *ibid.* **54**, 11169 (1996).
[32] The larger *average* deviation (averaged over all the III-V compounds) at the Γ point of the conduction band by LDA is mainly due to some narrow-band direct gap compounds. For instance, the deviation at the Γ point of the conduction band for GaSb is 65.8% with the band values of 0.0114 and 0.0189 eV by PAW and LMTO, respectively.
[33] W. Drube, D. Straub, and F. J. Himpsel, Phys. Rev. B **35**, 5563 (1987).